



# Reliability prediction of alkali-activated mortar during flexural loading using Weibull analysis

Yuyun Tajunnisa<sup>a,\*</sup>, Mohammad Idris Rasuli<sup>b</sup>, Akifumi Yamamura<sup>c</sup>, Mitsuhiro Shigeishi<sup>d</sup>

<sup>a</sup> Department of Civil Infrastructure Engineering, Institut Teknologi Sepuluh Nopember, Indonesia

<sup>b</sup> Independent Researcher, 6-17-2 Kurokami Chuo-Ku, Kumamoto, 860-0862, Japan

<sup>c</sup> Nippon Koei Co., Ltd., 5-4 Kojimachi, Chiyoda-ku, Tokyo, 102-8539, Japan

<sup>d</sup> Faculty of Advanced Science and Technology, Kumamoto University, Japan

## ARTICLE INFO

### Keywords:

Reliability  
Weibull analysis  
Alkali-activated materials  
Fracture process  
Carbon dioxide emission

## ABSTRACT

This study uses the Weibull analysis to predict the robustness of various mortars based on a fracture process analysis through a flexural test recorded by an acoustic emission sensor. Alkali-activated materials (AAMs) are an alternative to Portland cement that can decrease the amount of emitted CO<sub>2</sub>. This study aimed to characterise and compare the properties of AAM cement mortars to those of the commonly used ordinary Portland cement (OPC) mortars using the Weibull distribution to clarify the reliability and robustness of the prepared AAM cements; four different AAM cement mortar compositions—with fly ash (F), ground-granulated blast-furnace slag (G), and microsilica (M) alkali activation (sodium hydroxide (NaOH) and sodium silicate (Na<sub>2</sub>SiO<sub>3</sub>))—were considered in this study. The fracture process under a flexural loading of AAMs was based on four combinations of F/G/M activated by the alkaline solution—AAM-IV, AAM-V, AAM-VI, and AAM-VII, with OPC as control. The Weibull analysis showed that AAMs were more robust than the OPC mortar and possessed minor fractures compared to the OPC mortar.

## 1. Introduction

Ordinary Portland cement (OPC) is not environmentally friendly, considering it is responsible for 8 % of the overall CO<sub>2</sub> emissions worldwide [1]. Alkali-activated materials (AAMs) are more environmentally friendly than OPC, emitting 70 % less CO<sub>2</sub> than OPC [2]. AAMs are produced when aluminium silicate materials, such as fly ash and slag, react with an alkali source; such materials have binding characteristics [3,4]. Sodium hydroxide and sodium silicate are two prominent activators that are more available and usually used in AAM fabrication [5]. However, using sodium hydroxide results in higher alkalinity compared to using sodium silicate; moreover, sodium silicate contributes to the development of mechanical strength because it provides an additional silica to the (C–S–H) gel [6].

AAMs have extraordinary properties, such as superior mechanical strength [7], resistance against fire and acid [8,9], low drying shrinkage [10], and good workability [11].

Acoustic emission (AE), a non-destructive evaluation (NDE) method, has been used to identify activities inside materials [12]. Most AE tests are applied to detect material failure, including the material fracture process, considering the characteristics of AE parameters

\* Corresponding author.

E-mail address: [yuyun\\_t@ce.its.ac.id](mailto:yuyun_t@ce.its.ac.id) (Y. Tajunnisa).

<https://doi.org/10.1016/j.heliyon.2023.e21512>

Received 18 January 2023; Received in revised form 18 September 2023; Accepted 23 October 2023

Available online 30 October 2023

2405-8440/© 2023 The Authors. Published by Elsevier Ltd. This is an open access article under the CC BY-NC-ND license (<http://creativecommons.org/licenses/by-nc-nd/4.0/>).

correlate with a fracture [13]. One of the AE parameters used in this study is hit, which indicates AE activity by analysing the calculated number of hits for the accumulated hit values [14].

Weibull analysis is a method used to determine reliability characteristics using a relatively small sample size of the test data. The set data distribution is used to analyse specimen reliability and estimate its quality by investigating failure probability [15].

The Weibull analysis is beneficial because it does not require many samples. AE data is used to observe fracture growth in the specimen when a load is applied until the final failure. Data of AE hits indicate the cracks occurring inside the specimens, with crack accumulations causing failures. The failure rate is proposed to be analysed using the Weibull distribution to evaluate the fracture process of mortars under loading.

The reliability of recycled OPC concrete has been previously studied [16]. This study used AE data and applied Weibull's equation for evaluating reliability. The Weibull shape parameter  $m$  plays a major role in identifying the robustness of a material. A higher  $m$  indicates low AE activity at lower stress, implying that reliability increases with the increment in  $m$ .

Fractures of cement specimens have been studied through AE and ultrasonic techniques (UTs) [17]. The operation mechanisms of the AE and ultrasonic pulse velocity (UPV) methods are complementary; the UPV method cannot detect small cracks, but the AE method can identify cracks propagating in cement specimens during loading tests, while an inactive crack (without AE activity) can be detected with UPV. The simultaneous application of AE and UT identifies the time and location of cracks and provides a general assessment of material damage conditions [17]. The basis of acoustic monitoring and development using AE and UTs for concrete assessment has been previously presented [18]. This assessment includes the damage mode, content and severity of heterogeneity, and projection of the highest power. This field of acoustic monitoring helps substantially in monitoring the health of a structure; however, this study used only AE. An energy-dispersive X-ray spectroscopy (EDS) test was used to confirm the microstructures of the mortars. Considering the proposed method uses only a small number of samples, Weibull analysis is applied to predict the cementitious quality during fracture behaviour under flexural loading.

Nonetheless, using the Weibull distribution for observing fractures under flexural loading to clarify the reliability of variations in alkali-activated microsilica/slag/fly ash mortars (AAMs) and OPC mortar has not been discussed. This study aimed to investigate the fracture process reliability during a flexural test on four compositions of AAM cement and OPC in mortar specimens using Weibull analysis. In addition to studying the mechanical properties of the mortars, we explore the Weibull model parameter to predict the fracture behaviour in various mortar types of AAMs by a flexural test and compare it to that of the tested OPC, followed by a displacement test. The procedure to study the reliability is proposed based on the robustness methodology using the Weibull modulus  $m$ . This method calibrates the flexure load stress parameters recorded with AE and processed by the Weibull distribution and then predicts the robustness distribution for fractured specimens under flexural loading.

## 2. Experimental section

### 2.1. Materials and mixtures

The specimens used in this study were prismatic mortars with dimensions of  $40 \times 40 \times 160 \text{ mm}^3$ . The materials were OPC [19] based on Reference [20], Japanese fly-ash (F) type II [21], ground-granulated blast-furnace slag (GGBFS or G), and microsilica (M) [22]. The fine aggregate was standardised sand [23,24]. The chemical compositions of these materials were analysed by X-ray fluorescence (XRF), with details on their chemical compositions and specific densities presented in Table 1.

Four mixtures of AAMs were used to determine the fracture during the flexural test using an AE Weibull analysis, with sample proportions presented in Table 2. Several AAMs—I to VII—were considered for a study [25]. However, only the reliabilities of samples AAM-IV, AAM-V, AAM-VI, and AAM-VII—containing different percentages of microsilica (5, 10, 15, and 20 %, respectively)—were analysed in this study, with an OPC mortar used as a reference or control sample. In addition to comparing the AAM to the control sample, the influence of the microsilica on the reliability of these materials was studied.

The flexural loading test was conducted using three prismatic specimens for each mixture, as shown in Fig. 1. Cylindrical specimens with dimensions of  $50 \times 100 \text{ mm}^2$  were fabricated to determine compressive strength vs. displacement characteristics.

The alkaline solution consisted of 8-M sodium hydroxide (NaOH) and 56 % sodium silicate gel. The sodium silicate comprised 36 %  $\text{SiO}_2$ , 18 %  $\text{Na}_2\text{O}$ , and 46 %  $\text{H}_2\text{O}$ . All the samples had a fixed alkali solution concentration dosage, with a sodium silicate to sodium

**Table 1**  
Specific gravities (SGs) and oxide compositions of materials in weight percentage.

Material	Oxide composition (wt.%)							SG (g/cc)
	$\text{SiO}_2$	$\text{Al}_2\text{O}_3$	$\text{Fe}_2\text{O}_3$	CaO	$\text{Na}_2\text{O}$	$\text{H}_2\text{O}$	$\text{K}_2\text{O}$	
Fly ash (F)	55.19	25.35	7.57	4.06	–	–	–	2.33
GGBFS (G)	35	16	0.7	46	–	–	–	2.89
Microsilica (M)	93.67	0.83	1.3	0.31	0.4	–	–	2.22
Standardised sand	98.4	0.41	0.36	0.16	0.01	<0.2	0.01	2.64
OPC								3.16
Sodium silicate gel								1.6
Sodium hydroxide sol								1.22
Air entraining agent								1

**Table 2**  
Proportions and mechanical properties of AAM samples.

Sample	Solid precursor proportion	Fly ash (%)	GGBFS (%)	Microsilica (%)	Density (kg/m <sup>3</sup> )	Flexural strength (MPa)
AAM-IV	F <sub>47.5</sub> G <sub>47.5</sub> M <sub>5</sub>	47.5	47.5	5	2264	6.7
AAM-V	F <sub>45</sub> G <sub>45</sub> M <sub>10</sub>	45	45	10	2254	7.5
AAM-VI	F <sub>42.5</sub> G <sub>42.5</sub> M <sub>15</sub>	42.5	42.5	15	2222	8.9
AAM-VII	F <sub>40</sub> G <sub>40</sub> M <sub>20</sub>	40	40	20	2208	9.5
OPC	Control				2258	8.4

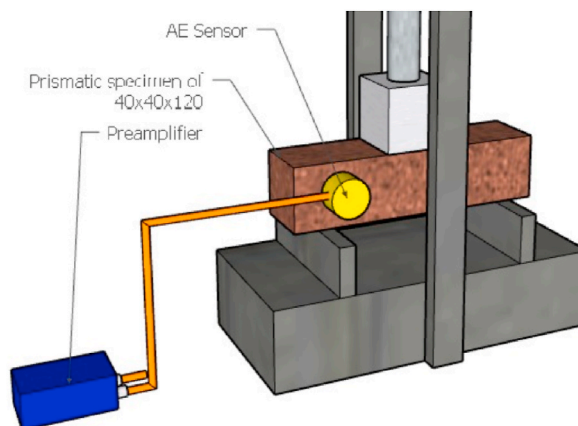


**Fig. 1.** AE setup in the flexural test.

hydroxide ratio of 1.5 [26,27]. The precursors (fly ash, GGBFS, microsilica) were mixed with the alkali solution and fine aggregate and compacted, cured, and demoulded [8].

AAM mixtures (887.8 cc) were mixed in a 2-L batch mixer in a control room at 18–20 °C at a relative humidity (RH) of 30–50 %. Raw precursors were mixed for 2 min at a low speed. The 8 M sodium hydroxide solution, previously dissolved at least one day before the mortar mixing, was mixed manually with the sodium silicate gel for 5 min followed by 10 min of rest before the AE agent was added. This alkaline liquid was then added and mixed with the raw precursors for 2 min at a low speed. The mixer was stopped, standardised sand was added, and low-speed mixing was conducted again for another 3 min. After mixing each mixture, the mortars were immediately cast into three prism moulds (40 × 40 × 160 mm<sup>3</sup>) or cylindrical moulds (50 × 100 mm<sup>3</sup>). The moulds were compacted on a vibrator table for 2 min to remove air bubbles. The specimens were cured in air at 18–20 °C and RH of 30–50 %, sealed with plastic, demoulded after 6 d, and then continued to be air-cured under unsealed conditions up to the testing date. For the OPC mortar, the mixing process was conducted according to Ref. [23].

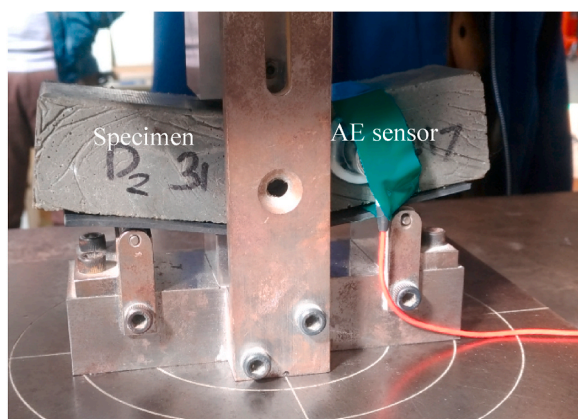


**Fig. 2.** Flexural and AE tests on the prismatic specimen after failure.

2.2. Testing method

The AE test on the prismatic specimens was performed on the 28th day during flexural loading. Figs. 1 and 2 show the detailed setup of the AE test. A wideband UT-1000 AE sensor, with good frequency response between 100 and 1000 kHz and stable against fluctuations in environmental parameters, was attached to the span of the specimen surface using an epoxy material. The output voltage of the AE sensor was on the order of millivolt or below. Therefore, a preamplifier and postamplifier were required to enlarge the signal of the AE system, with the AE signals of this experiment amplified at 40 dB. The threshold level was also set at 40 dB to reduce the environmental noise, with the signals recorded under one-channel monitoring. The MISTRAS non-destructive test system employed AE measurements, with the specimens evaluated at zero load until they reached failure. The maximum flexural strength applied to the specimen was set at 20 kN, corresponding to 5 kV, while 1 kV corresponded to 4 kN.

3. Results and discussion

3.1. Mechanical properties of a hardened mortar

Incorporating GGBFS and microsilica influences AAMs’ mechanical properties as a fly ash replacement in an alkali-activated mortar [25].

The AAM containing 15–20 % microsilica had higher flexural strength than the OPC mortar, with the highest flexural strength (9.5 MPa) obtained for AAM VII with the highest M content. Other studies also confirmed the modification of flexural strength by microsilica [28], attributed to its pozzolanic behaviour and high silica content, which improves the bond of the paste and increases strength and durability [29]. Moreover, microsilica acts as a filling agent, filling the spaces throughout the sample, which increases material strength [30]. This finding is consistent with the study results obtained by Li et al. [31], who found that silica (Si) participates in the reaction process of AAMs and that Si/Al influences strength development in a low-calcium system.

Table 2 presents the proportions of mortars and properties of hardened mortars (28-day old). The density of AAM VII, compared to other AAMs (2222–2264 kg/m<sup>3</sup>), is slightly lower (2208 kg/m<sup>3</sup>) and lower than that of OPC (2258 kg/m<sup>3</sup>), as shown in Table 2, implying that mortar density, for both AAM and OPC, typically around 2200 kg/m<sup>3</sup>, is almost equivalent to the density designation of mortars, approximately 2300 kg/m<sup>3</sup>.

EDS tests were conducted on two sample types—AAM-IV and AAM-VII, with EDS used to determine their chemical compositions. Fig. 3 (a) shows elemental analysis through SEM-EDX of AAM-IV. An example of an AAM-IV graphic containing the dominant element Si, followed by O, Ca, Al, Na, Mg, and Fe, is seen in Fig. 5 (a). Furthermore, Fig. 4 (a) shows that the dominant elements were Si and O, followed by Al, Ca, Na, Mg, and Fe; these EDS results are also shown in the table in Fig. 5 (b). Fig. 5 (a) and (b) show the raw components for AAM-IV and VII. The EDS results are for AAM-VII with a Si content higher by 3.75 % and Ca content higher by 0.46 % [wt.%]. A scanning electron microscopy SEM–EDS image with a magnification of 0.5k shows a C–N–A–S–H gel of AAM, the main reaction product. AAM-VII exhibited a better ductile mixture as an SEM-EDS test result than AAM-IV, as shown in Fig. 3 (b) and 4 (b). Fig. 3 (b) shows that the EDS image of AAM-IV contains wider and longer connected cracks appearing on the AAM surface, whereas Fig. 4 (b) shows different crack patterns on the AAM-VII surface with tiny and short cracks. AAM-VII has ductile materials with higher Si and Ca contents than those of AAM-IV.

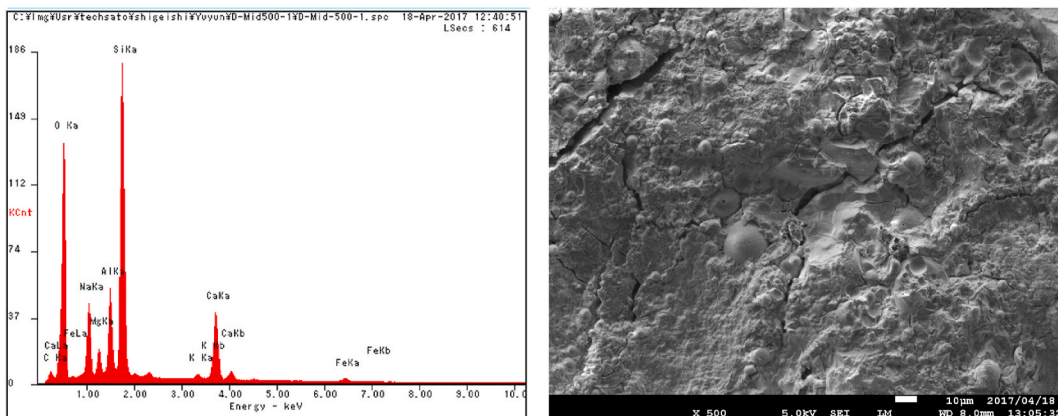


Fig. 3. Elemental ED spectrum and quantification results of AAM-IV (a) Elemental Analysis through EDS of AAM-IV (b) SEM image of AAM-IV (0.5k).

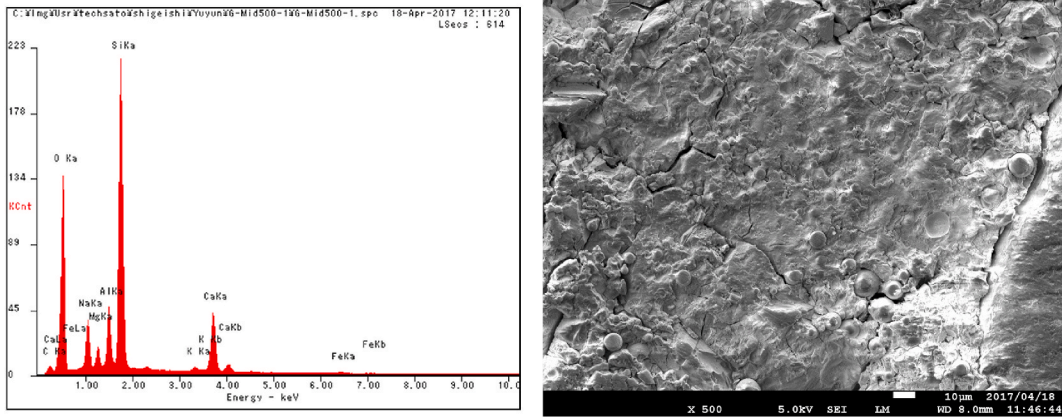


Fig. 4. Elemental ED spectrum and quantification results of AAM-VII (a) Elemental Analysis through EDS of AAM-VII (b) SEM image of AAM-VII (0.5k).

Element	Wt%	At%
CK	4.63	8.06
OK	40.04	52.35
NaK	6.97	6.35
MgK	2.03	1.75
AlK	7.01	5.43
SiK	26.05	19.40
KK	0.78	0.42
CaK	10.65	5.56
FeK	1.83	0.69
Matrix	Correction	ZAF

(a)

Element	Wt%	At%
CK	3.98	6.98
OK	40.27	52.95
NaK	5.56	5.08
MgK	1.87	1.62
AlK	5.76	4.49
SiK	29.80	22.32
KK	0.69	0.37
CaK	11.11	5.83
FeK	0.96	0.36
Matrix	Correction	ZAF

(b)

Fig. 5. EDS element contents in (a) AAM-IV (0.5k) and (b) VII (0.5k).

3.2. Fracture process of AAM specimens obtained by AE hits under a flexural stress loading

AE generation is related to deterioration [32], with AE events observable under loading when samples experience additional microcracks causing failures. A low-stress level, a lower-quality specimen mixture generates high AE. In contrast, AE generation indicates higher specimen quality for a low value initially. In this study, we propose that the failure rate corresponds to the cumulative AE hit occurrence; discovering an AE hit indicated the occurrence of cracks inside the specimen, with crack accumulation triggering specimen failure. The failure rate was then analysed using the Weibull distribution to evaluate the specimen quality. The cement

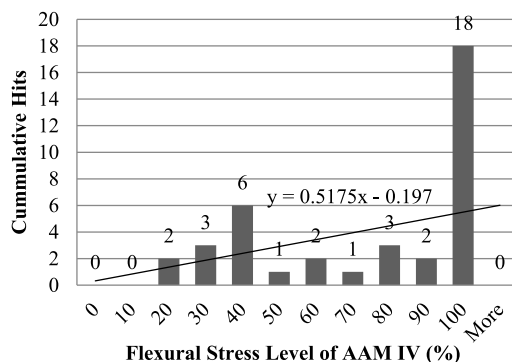


Fig. 6. Cumulative hits vs. stress level of an exemplary specimen of AAM-IV.

quality in the mortar is based on the probability of crack occurrence at each stress level until the specimen fails under flexural loading.

The correlation between the stress level and number of AE hits is presented in Figs. 10 and 11. Fig. 10 shows an example of the fracture process according to the relationship of the AE hits vs. the stress level in AAM-IV, which contains 5 % M. The graph presents small AE activities during the initial (stress level = 0–33 %) and middle (stress level = 33–67 %) stages under the flexural loading test, with AE activity significantly increasing during the final stage. This behaviour reveals that the fracture process on the AAM-IV specimen includes several microcracks, which occur at the final phase of the first stage (stress level of approximately 33 %) or the beginning of the middle stage. The crack continues expanding during the middle stage (at a stress level range of 33–67 %). Finally, AAM-IV reaches failure during the final loading stage (stress level of 67–100 %). Fig. 6 presents an example of the fracture process according to the relationship of AE hits vs. flexural stress level of an exemplary specimen of AAM-VI containing 15 % micro silica. The AE activity during the initial stage (stress level of approximately 0–33 %) was zero. In the middle stage, at the beginning (stress level = 33–76 %), slight AE activities appeared when the flexural stress was approximately 35 %; in the final stress stage, the AE activities increased significantly.

Fig. 7 results imply that the AAM-VI fracture process did not include cracks during the first loading stage, with slight microcracks merging into bigger cracks during the middle stage. Finally, AAM-VI experienced the failure point during the final stage of the flexural loading test. A higher AE amplitude at large numbers in the AAM-VI specimen indicates a faster crack growth before failure.

The above results reveal that the AAM-VI mortar possesses a better or more ductile, less brittle, or more robust behaviour than AAM-IV, as shown in Figs. 6 and 7, with the cracks growing inside the AAM following the trend of flexural strength level. The flexural strength of AAM-VI (8.9 MPa) was higher than that of AAM-IV (6.7 MPa), further implying that the flexural strength of the mortar is suitable for the fracture process of the specimen.

### 3.3. Probability of failure during flexural loading evaluated by the Weibull distribution

The flexural strength (%) is denoted by  $x$ , the Weibull distribution contributes with a distribution for the failure rate,  $f(x)$  is the cumulative number of AE hits at  $x$ ,  $m$  is the Weibull shape parameter, and  $\beta$  is the Weibull scale parameter. The cement type quality is defined by

$$1 - f(x) = e^{-\left[\frac{x}{\beta}\right]^m}$$

$m$  is termed as slope according to its graph. The shape parameter ( $m$ ) indicates the type of failure based on the slope. If  $m < 1$ , high AE activities are generated at a low-stress level;  $m = 1$  shows a constant failure rate, indicating a random failure. When  $m > 1$ , the failure rate generally increases with time, but the AE and fracture occurrence are less likely at a low-stress level. Therefore, the reliability of a material increases with  $m$  [33].

Figs. 8–13 present different Weibull distribution parameters to evaluate the qualities of various mixtures of specimens.

Fig. 8 shows the probability of failure during flexural load of three AAM-IV specimens with different amplitude filter values, which are Fig. 8 (a) amplitude filter larger than 40, Fig. 8 (b) larger than 50, and Fig. 8 (c) larger than 60 dB. Fig. 8 (a) shows AAM-IV (with amplitude filter values larger than 40) on three specimens of AAM-IV-1, AAM-IV-2, and AAM-IV-3 have a slight difference in the gradient ( $m$ ): 1 (1.98), 2 (2.44), and 3 (3.53), indicating that AAM-IV-1, as shown in Fig. 8 (a), AAM-IV-2 in Fig. 8 (b), and AAM-IV-3 in Fig. 8 (c), have similar failure probabilities during the flexural loading test.

Fig. 9 shows the probability of failure during flexural load of three AAM-V specimens with three different amplitude filter values, which are larger than 40 in Fig. 9 (a), 50 in Figure (b), and 60 dB in Fig. 9 (c). Fig. 9 shows AAM-V, which has a higher gradient when the amplitude is higher. In AAM-V-2, gradient values of 5.64, 106.6, and 98.79 were achieved when amplitude filters larger than 40, 50, and 60 dB were used, respectively. The high gradient indicates that AAM-V-2 had the lowest failure probability in the flexural test.

The exact circumstances applied for AAM-VI and AAM-VII are shown in Figs. 10 and 11. The Weibull gradients had slight differences when the amplitude filter value was higher than 40 dB, whereas the values had more significant differences when the filter amplitude value was higher than 50 or 60 dB, indicating that the cracks that occurred at the initial stage of the stress were extremely small and thin or that environmental noise may have influenced the procedure. Fig. 10 (a), (b), and (c) present failure probability when a flexural load of three specimens of AAM VI, each with three amplitude filter values larger than 40, 50, and 60 dB. Fig. 11 shows the failure probability of AAM VII, which has higher microsilica content and lower slag-fly ash content than other AAMs. Fig. 11 (a), (b), and (c) apply AAM VII for three amplitude filter values larger than 40, 50, and 60 dB, respectively. Figs. 8–11 evaluate the qualities of various mixtures by studying AAMs' probability of failure during flexural load with different amplitude filter values.

Fig. 12 (a), (b), and (c) show the gradients of the OPC specimens obtained by the AE test with filter amplitudes larger than 40, 50, and 60 dB. The overall result of the OPC test shows that each specimen has a similar average gradient, regardless of the filter AE amplitude. The lower  $m$  indicates that the prisms of the OPC mortars have a higher failure probability than those of the AAMs under the flexural loading test, owing to the relatively small gradient.

A filter amplitude higher than 50 dB is most suitable for determining the fracture process of various mortars during flexural loading tests using AE. In contrast, 40 dB AE is considered environmental noise because it shows a low impact during the initial test; therefore, the 40 dB AE filter amplitude is unsuitable for this research. The material cracks growing inside AAMs are consistent with the result of the flexural strength.

Fig. 13 (a) and (b) summarise the overall Weibull parameters of AE hits of various mixtures during the flexural test using two filter amplitudes higher than (a) 50 and (b) 60 dB. Macrocracks cause specimen failure when the amplitude is higher than 50 or 60 dB. The

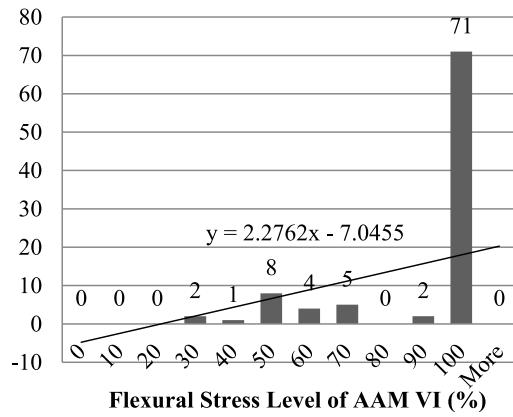


Fig. 7. Cumulative hits vs. stress level of an exemplary specimen of AAM-VI.

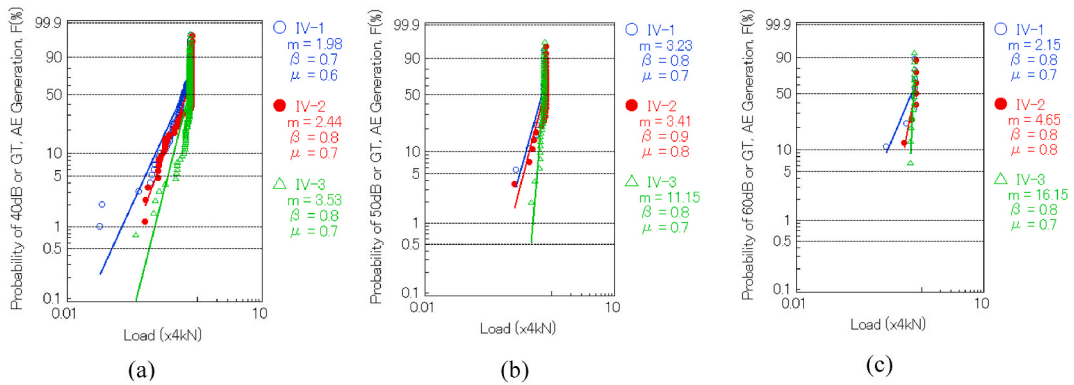


Fig. 8. Probability of failure during flexural loading of three AAM-IV specimens with amplitude filter values larger than (a) 40, (b) 50, and (c) 60 dB.

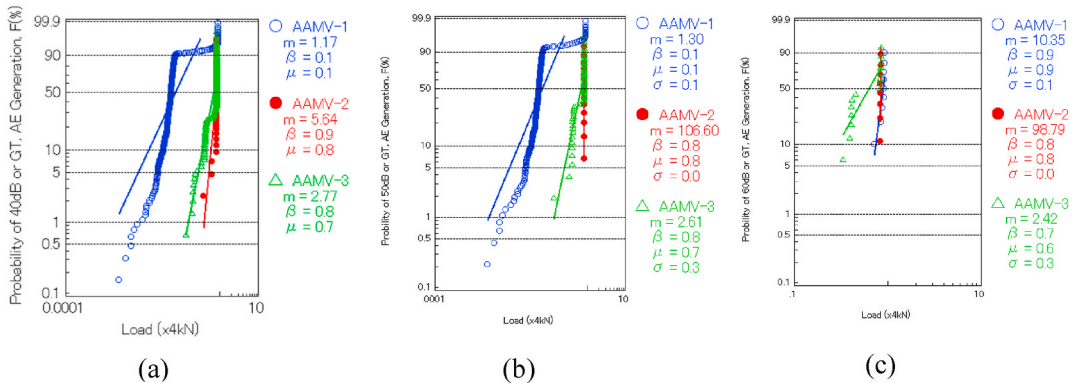


Fig. 9. Probability of failure during flexural loading of three AAM-V specimens with amplitude filter values larger than (a) 40, (b) 50, and (c) 60 dB.

highest gradient was achieved by AAM-VII (FA40G40M20) for specimen 3 at 5.94, using a filter amplitude higher than 50 dB. This result suggests that AAMs containing more microsilica exhibit more ductile behaviours in the fracture process than AAMs (AAM-IV, V, and VI) with less microsilica. According to the Weibull analysis using a filter amplitude higher than 50 dB, the most ductile mixture is AAM-VII, followed by AAM-IV, VI, V, and OPC mixtures. The AAMs have ductile, better, or robust behaviours in the fracture process and a lower probability of failure due to flexural strength than OPC.

This study validates previous findings [34], where the reliability of the AAM mortars was higher than that of an OPC mortar under compressive loading.

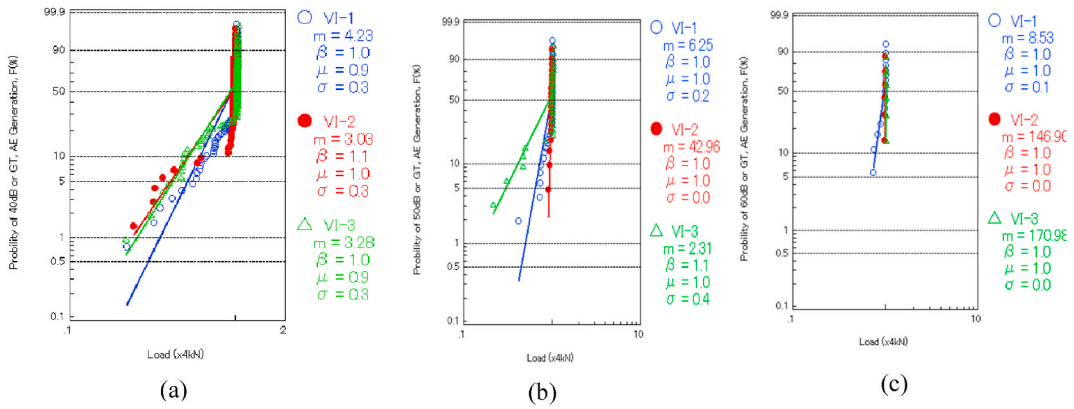


Fig. 10. Probability of failure during flexural loading of three AAM-VI prisms with amplitude filter values larger than (a) 40, (b) 50, and (c) 60 dB.

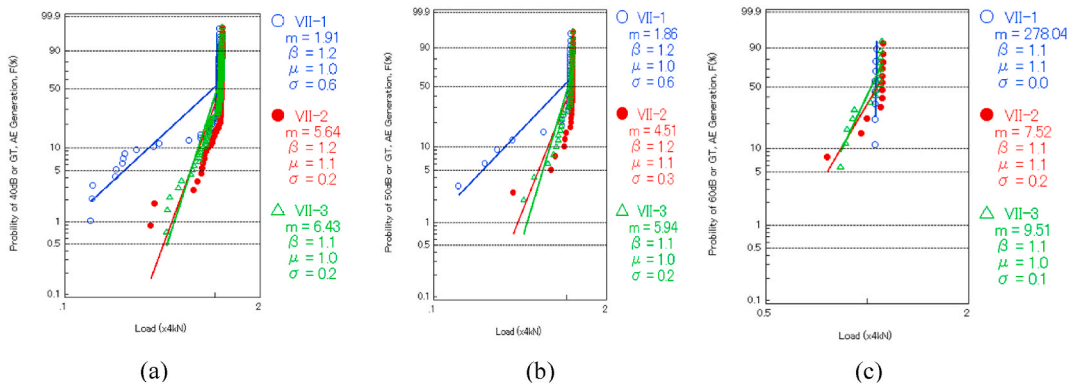


Fig. 11. Probability of failure during flexural loading of three AAM-VII prisms with amplitude filter values larger than (a) 40, (b) 50, and (c) 60 dB.

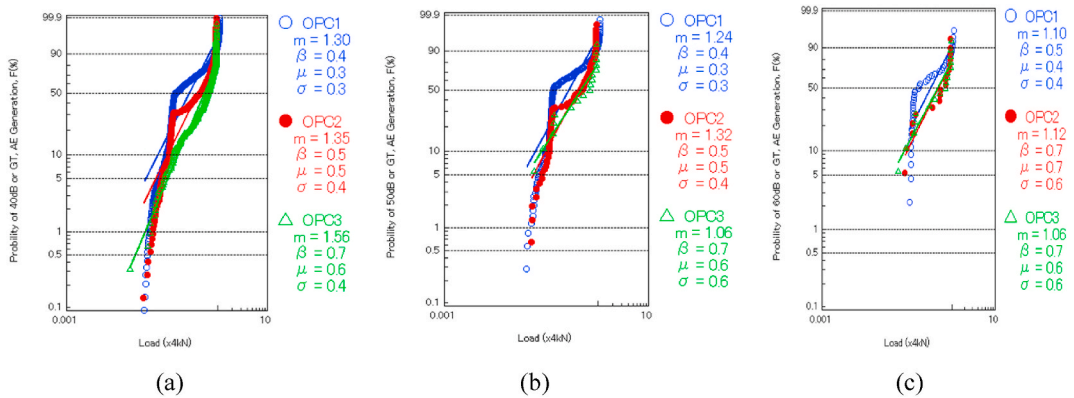


Fig. 12. Probability of failure during flexural loading of three OPC specimens with amplitude filter values higher than (a) 40, (b) 50, and (c) 60 dB.

3.4. Compressive strength vs. displacement

Fig. 14 shows the compressive strength vs. displacement curves of AAMs and OPC, revealing that AAMs have a slightly longer displacement than OPC. Displacement tests were conducted to assess the ductility of the specimen mortar containing mixed variations. The AAMs exhibited long deflections after the maximum strength. The graph indicates that the AAMs are more ductile in the fracture process than the OPC mortar, confirming the reliability test result obtained through the Weibull distribution.

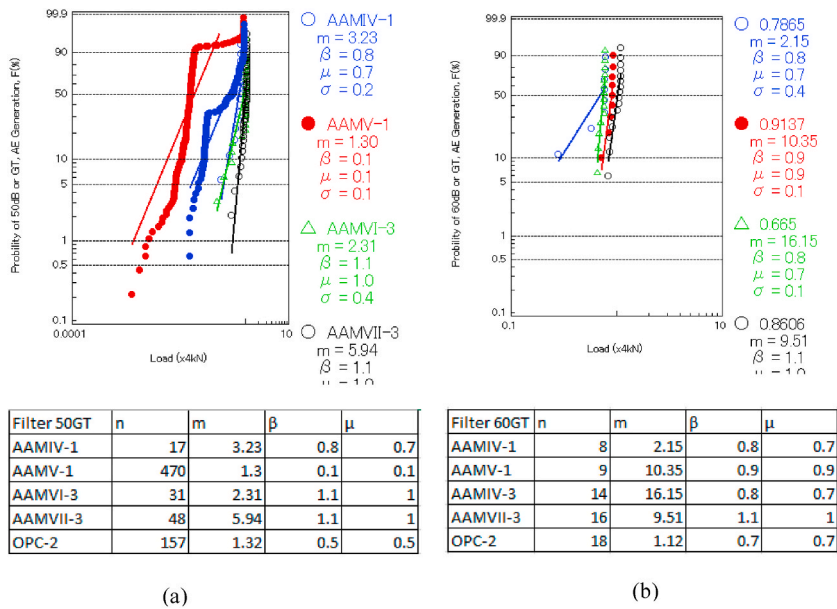


Fig. 13. AAMs and OPC mixtures with filter amplitudes larger than (a) 50 and (b) 60 dB.

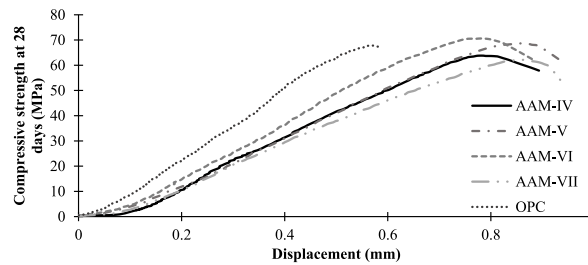


Fig. 14. Compressive strength vs. displacement curves of specimens.

4. Conclusion

We investigated the fracturing mechanism on four-composition AAMs and one-composition OPC mixtures using the AE–Weibull analysis method during a flexural loading test. The AE activities inside the AAMs were considerably lower at the initial loading and increased at the later stages. The reliability test showed that AAMs are more robust and reliable than OPC mortars. The ductility and robustness of the samples increased with the addition of microsilica. The microstructure and compressive strength vs. displacement characteristics corroborated the higher ductility of the AAMs, confirming the reliability test result.

Author contribution statement

Yuyun Tajunnisa: Conceived and designed the experiments; Performed the experiments; Analysed and interpreted the data; Contributed reagents, materials, analysis tools, or data; Wrote the paper. Mohammad Idris Rasuli: Analysed and interpreted the data; Contributed reagents, materials, analysis tools, or data; Wrote the paper. Akifumi Yamamura: Performed the experiments. Mitsuhiro Shigeishi: Conceived and designed the experiments.

Data availability statement

Data will be made available on request.

Declaration of competing interest

The authors declare that they have no known competing financial interests or personal relationships that could have appeared to influence the work reported in this paper.

## Acknowledgement

This research was conducted at Kumamoto University, Japan, supported by The Hitachi Global Foundation Ref. RS-15, E-1 March 8, 2019, Kumamoto University, and Institut Teknologi Sepuluh Nopember, Surabaya, Indonesia.

## References

- [1] R.M. Andrew, Global CO<sub>2</sub> emissions from cement production, *Earth Syst. Sci. Data Discuss.* (2019) 1675–1710, <https://doi.org/10.5194/essd-2019-152>.
- [2] A. Heath, K. Paine, M. McManus, Minimising the global warming potential of clay based geopolymers, *J. Clean. Prod.* 78 (2014) 75–83.
- [3] V.D. Glukhovskiy, I.A. Pashkov, G.A. Yavorsky, New Building Material, in Russian, *Bulletin of Technical Information, GlavKievStroy*, Kiev, 1957.
- [4] J. Davidovits, Synthetic mineral polymer compound of the silicoaluminates family and preparation process, U.S. Patent 4 (472) (1984) 199.
- [5] A. Palomo, M.W. Grutzeck, M.T. Blanco, Alkali-activated fly ashes. A cement for the future, *Cement Concr. Res.* 29 (8) (1999) 1323–1329, [https://doi.org/10.1016/S0008-8846\(98\)00243-9](https://doi.org/10.1016/S0008-8846(98)00243-9).
- [6] T. Phoo-ngernkham, A. Maegawa, N. Mishima, S. Hatanaka, P. Chindaprasirt, Effects of sodium hydroxide and sodium silicate solutions on compressive and shear bond strengths of FA–GBFS geopolymer, *Construct. Build. Mater.* 91 (2015) 1–8.
- [7] M.I. Rasuli, A study on the influence of sodium silicate concentration and SiO<sub>2</sub>: Na<sub>2</sub>O ratio on the properties of low-calcium fly ash-based alkali-activated materials cured at ambient condition, *Adv. Mater. Sci. Eng.* 2022 (2022), <https://doi.org/10.1155/2022/7762507>. Article ID 7762507, 7 pages, 2022.
- [8] K. Kupwade-Patil, E.N. Allouche, Impact of alkali-silica reaction on fly ash-based geopolymer concrete, *J. Mater. Civ. Eng.* 25 (2013) 131–139, [https://doi.org/10.1061/\(ASCE\)MT.1943-5533.0000579](https://doi.org/10.1061/(ASCE)MT.1943-5533.0000579).
- [9] H. Rashidian-Dezfouli, R.P. Rao, Study on the effect of selected parameters on the alkali-silica reaction of aggregate in ground glass fiber and fly ash-based geopolymer mortars, *Construct. Build. Mater.* 271 (2021).
- [10] J.L. Provis, G.C. Lukey, van Deventer, Jsj, Do geopolymers contain nanocrystalline zeolites? A reexamination of existing results, *Chem. Mater.* 17 (12) (2005) 3075–3085.
- [11] M.I. Rasuli, Y. Tajunnisa, A. Yamamura, M. Shigeishi, A consideration on the one-part mixing method of alkali-activated material: problems of sodium silicate solubility and quick setting, *Heliyon* 8 (1) (2022), e08783, <https://doi.org/10.1016/j.heliyon.2022.e08783>. January 2022.
- [12] C. Grosse, Introduction, in: *Acoustic Emission Testing Basic Research - Applications in Civil Engineering*, Springer, Berlin, 2008, pp. 3–10.
- [13] M. Ohtsu, Fundamentals and applications of acoustic emission, *Short Course 101-1111-00L* (2007).
- [14] A. Behnia, H.K. Chai, T. Shiotani, Review Advanced structural health monitoring of concrete structures with the aid of acoustic emission, *Construct. Build. Mater.* 65 (2014) 282–302.
- [15] R. Arbernethy, An overview of Weibull analysis, in: *The New Weibull Handbook*, Florida, 2002, pp. 1–11.
- [16] KNi Nyoman, L. Shinya, M. Shigeishi, Fracture process and reliability of concrete made from high grade recycled aggregate using acoustic emission technique under compression, *Mater. Struct.* 46 (2013) 1441–1448.
- [17] G. Dimitros, Aggelis, T. Shiotani, S. Momoki, A. Hiram, Acoustic emission and ultrasound for damage characterization of concrete elements, *ACI Mater. J.* 106 (6) (2009). Title no. 106-M56.
- [18] D.G. Aggelis, A.C. Mpalaskas, T.E. Matikas, Acoustic Monitoring for the Evaluation of Concrete Structures and Materials, *Acoustic Emission and Related Non-destructive Evaluation Techniques in the Fracture Mechanics of Concrete, Fundamentals and Applications*, Woodhead Publishing Series in Civil and Structural Engineering, 2015, pp. 269–286.
- [19] ISO 679, Cement - Test Methods - Determination of Strength, 2009.
- [20] R.5210 Jis, Standard for Portland Cement, 2009.
- [21] A.6201 Jis, Fly Ash for Use in Concrete, 2015.
- [22] A.6207 Jis, Silica Fume for Use in Concrete, 2016.
- [23] R.5201 Jis, Physical Testing Methods for Cement, 2015.
- [24] I-12 Cajs, Chemical Analysis, Association Japan Cement, 1981.
- [25] Y. Tajunnisa, M. Sugimoto, T. Uchinuno, T. Sato, Y. Toda, A. Hamasaki, T. Yoshinaga, K. Shida, M. Shigeishi, Performance of alkali-activated fly ash incorporated with GGBFS and micro-silica in the interfacial transition zone, microstructure, flowability, mechanical properties and drying shrinkage, *Green Construction and Engineering Education for Sustainable Future* 1887 (2017).
- [26] Y. Tajunnisa, M. Sugimoto, T. Sato, M. Shigeishi, A study on factors affecting geopolymerization of low calcium fly ash, *Int. J. GEOMATE* 13 (36) (2017) 100–107.
- [27] Y. Tajunnisa, M. Sugimoto, T. Uchinuno, T. Sato, T. Toda, A. Hamasaki, T. Yoshinaga, K. Shida, M. Shigeishi, Effect of GGBFS and micro-silica on mechanical properties, shrinkage and microstructure of alkali-activated fly ash mortar, *Int. J. GEOMATE* 13 (39) (2017) 87–89.
- [28] M. Shafieyzadeh, Prediction of flexural strength of concretes containing silica fume and styrene-butadiene rubber (SBR) with an empirical model, *J. Inst. Eng. India Ser. A* 96 (2015) 349–355, <https://doi.org/10.1007/s40030-015-0140-0>.
- [29] S. Chandra, L. Berntsson, 9 - use of silica fume in concrete, 1996, in: Satish Chandra, *Waste Materials Used in Concrete Manufacturing*, William Andrew Publishing, 1996, pp. 554–623, <https://doi.org/10.1016/B978-081551393-3.50012-0>, 9780815513933.
- [30] K. Behfarnia, M. Rostami, Effects of micro and nanoparticles of SiO<sub>2</sub> on the permeability of alkali activated slag concrete, *Construction and Building Materials, Construction and Building Materials* 131 (2017) 205–213.
- [31] N. Li, C. Shi, Q. Wang, Z. Zhang, Z. Ou, Composition design and performance of alkali-activated cements, *Mater. Struct.* 50 (2017) 178.
- [32] Ohtsu, AE in Concrete: Acoustic Emission Testing Basic Research - Applications in Civil Engineering, Springer, Berlin, 2008, pp. 221–238.
- [33] J. Seidel, N. Claussen, J. Rodel, Reliability of Alumina Ceramics: Effect of Grain Size, *Journal of European Ceramic Society*, 1995, pp. 395–404.
- [34] Y. Tajunnisa, M. Shigeishi, Bayuaji Ridho, M.S. Darmawan, Reliability of Alkali-activated and Portland Cement Mortar Under Compressive Test by Acoustic Emission 17 (60) (2019).